Supporting VO(acac)₂ and MoO₂(acac)₂ onto Amine and Imine-functionalized Natural Diatomite Nanoparticles: Efficient Catalysts for Epoxidation of Olefins Using TBHP

Sahar Asadi, Bahram Bahramian*, Vahid Mirdarvatan

Department of Chemistry, Shahrood University of Technology, Shahrood, Iran

Abstract: The natural diatomite nanoparticles (Dt) were covalently functionalized by 3-(trimethoxysilyl)-propylamine (MSPA) and salicylaldehyde to support VO(acac)₂ and MoO₂(acac)₂ precursor complexes. The prepared compounds were characterized by FT-IR, PXRD, SEM, EDX, ICP, and BET techniques. Then they were used to catalyze the heterogeneous epoxidation of *cis*-cyclooctene as a model alkene using tert-butyl hydroperoxide (TBHP). Various parameters that affect catalytic efficiency were investigated, and the optimized experimental conditions were successfully used for the epoxidation of other linear and non-linear alkenes. The important advantages of these new catalytic systems are their simple preparation, low catalyst loading, and high product yield. Moreover, these catalysts can be used up to three times for an efficient epoxidation of *cis*-cyclooctene.
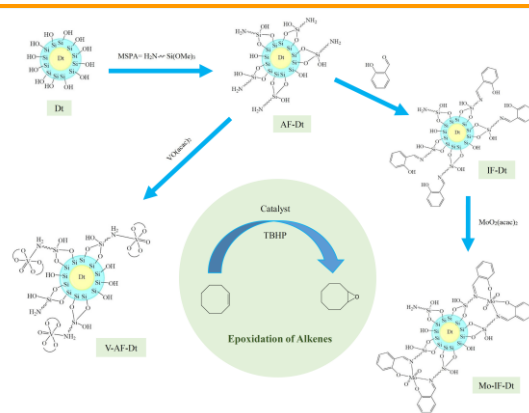
1. INTRODUCTION

Epoxides, one of the most known valuable precursors, play a key role in producing several commercially important chemicals and intermediates, as well as in the field of pharmacology.[1] Ethylene oxide and propylene oxide are two important commodity chemicals produced by the epoxidation of ethylene and propylene, respectively.[2] In recent years, various homogeneous[3-5] and heterogeneous[6-9] catalytic systems have been developed for epoxidation reactions. Most homogeneous catalytic systems consist of main group elements and transition metals. Amongst these, the early transition metals such as molybdenum and vanadium are of particular interest because they are stable in their highest oxidation state during the catalytic procedure.[10-14] The vanadium and molybdenum complexes have drawn much attention as catalysts in different oxidation reactions such as epoxidation of olefins, oxidation of sulfides to sulfoxides, hydroxylation of phenols, and oxidation of alcohols to aldehydes and ketones.[15-20] The high cost and toxicity are important challenges in the metal-containing catalytic systems. The immobilization of the metal ions onto insoluble supports can solve these problems and improve the efficiency of the catalyst.[21,22]

Diatomite (SiO₂.nH₂O) is one of the insoluble inorganic catalyst carriers. It is a siliceous sedimentary rock containing diatom formed at low temperature and pressure.[23-27] The silanol groups on the surface of diatomite are active and display a tendency to react with different functional groups.[28] Due to its high porosity, high specific surface area, high reusability, low density, and high chemical stability, the diatomite has been widely used as filter media,[29,30] filler,[31–33] absorbent,[34–37] and abrasive[38] material. There is great interest in using it as a catalyst carrier in various catalytic reactions such as carbonylation of amine,[39] nitration of toluene,[40] hydroxylation of phenol,[41] oxidative desulfurization,[42] oxidation of benzene,[43] hydrogenation of aliphatic esters,[44] Heck,[45] Suzuki,[46] and Sonogashira[47] reactions. Furthermore, metal-diatomite composites have been utilized as catalysts in photocatalytic degradation of gaseous formaldehyde,[48] rhodamine B,[49] methylene blue,[50] and ciprofloxacin[51]

Some years ago, we reported a diatomite-supported manganese(III) Schiff base complex, which exhibited significant catalytic activity for epoxidation of alkenes and hydroxylation of alkanes using sodium periodate as an oxidant.[52] As part of our continuing studies on the catalytic epoxidation of alkenes using V and Mo-

containing catalysts,[53-56] we herein prepare amine and imine-functionalized diatomite nanoparticles to support VO(acac)$_2$ and MoO$_2$(acac)$_2$ complexes, and study their catalytic activity in the epoxidation of alkenes using TBHP.

2. EXPERIMENTAL

All solvents and chemicals were purchased from commercial reagents and used without further purification. The natural diatomite was obtained from the Shahrood region in the north of Iran, and then purified by the method described in the literature.[36] For this purpose, the raw diatomite (1 g) was washed with 15 mL of HCl solution (2 M), and then heated at 105 °C for 4 h. The diatomite dispersion was centrifuged, and the resulting powder was washed with water. The acid-washing process was repeated until the diatomite was free of chloride anions as determined by AgNO$_3$. The precipitate was collected and dried at 80 °C overnight.

Characterization methods

Infrared spectra were measured with a Perkin-Elmer 521 spectrophotometer using KBr pellets. Powder X-ray diffraction was collected on a Bruker D8 Advance with Cu Kα irradiation. The morphology of the products was analyzed by a Zeiss Sigma 300-HV scanning electron microscope. The BET analysis was carried out on a Belsorp mini II apparatus (BEL, Japan) to obtain the surface area, pore volume, and pore size distribution of the support and the catalyst. Gas-liquid chromatography (GLC) experiments were carried out on a Gostar Faraz GC-2560 instrument using a 2-m column packed with silicon DC-200 or Carbowax 20 M. In the GLC tests, n-decane was used as an internal standard. The other operating parameters were as follows: injector temperature, 180 °C; detector temperature, 200 °C; oven temperature, 70-200 °C. The conversions and yields were calculated by normalizing the areas of the GC peaks by means of the area of the internal standard peak (n-decane).

Preparation of vanadium-supported amine-functionalized diatomite (V-AF-Dt)

To a solution of 3-(trimethoxysilyl)-propylamine (2 mL, 11.37 mmol) in dry toluene (50 mL) was added 1 g of pure diatomite (Dt) and refluxed for 20 h at 110 °C to yield the amine-functionalized diatomite (AF-Dt). The resulting white solid was isolated, washed twice with dry toluene, and left at 70 °C overnight. The AF-Dt was used to support the VO(acac)$_2$ precursor complex. To achieve this, a mixture of AF-Dt (0.3 g) and VO(acac)$_2$ (0.07 g, 0.26 mmol) was refluxed in ethanol (60 mL) for 12 h. The final mixture was centrifuged, washed with ethanol, and then dried at 60 °C to give the vanadium-supported amine-functionalized diatomite (V-AF-Dt) (Scheme 1).

Preparation of molybdenum-supported imine-functionalized diatomite (Mo-IF-Dt)

The imine-functionalized diatomite (IF-Dt) was prepared from the condensation reaction of AF-Dt (1 g) and salicylaldehyde (0.3 mL, 2.87 mmol) in ethanol (20 mL) for 15 h. The resulting product was filtered, washed with ethanol, and dried at 70 °C. The IF-Dt was used to support the MoO$_2$(acac)$_2$ complex. To achieve this, the MoO$_2$(acac)$_2$ (0.07 g, 0.21 mmol) was reacted

with IF-Dt (0.3 g) in ethanol (60 mL) under reflux conditions for 12 h. After centrifugation, the resulting solid was washed several times with ethanol, and then dried at 60 °C to afford the molybdenum-supported imine-functionalized diatomite (Mo-IF-Dt) (Scheme 1).
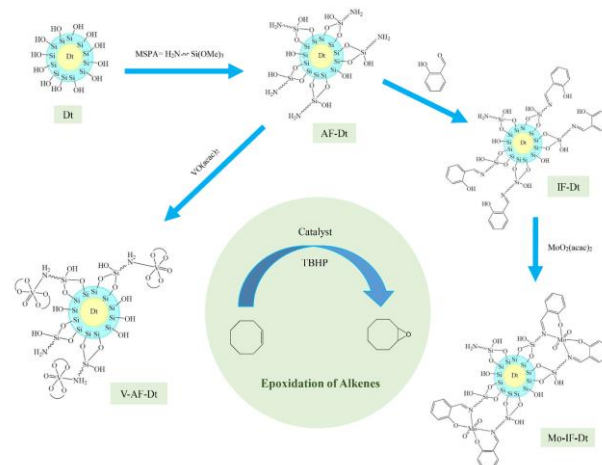
Scheme 1. Attempt to support VO(acac)$_2$ and MoO$_2$(acac)$_2$ on AF-Dt and IF-Dt

Catalytic epoxidation of alkenes

The *cis*-cyclooctene was employed as a model alkene in the catalytic epoxidation reactions using TBHP. A general procedure was used for all the reactions. First, a solvent was mixed with *cis*-cyclooctene, and then an oxidant was added to the solution. The prepared mixture was poured into a 25 mL round-bottom flask containing the catalyst, and then stirred for a certain time. The reactions were monitored by GLC equipped with a flame ionization detector. The alkene conversions and product selectivity were calculated using their peak areas by the standard addition method. After completing the reaction, the catalyst was recovered by centrifugation, washed with solvent, dried at 60 °C overnight, and used in the next cycle (Table 6).

3. RESULTS AND DISCUSSION

Preparation of catalysts

The natural diatomite nanoparticles (Dt) were covalently functionalized with MSPA to generate the amine-functionalized diatomite (AF-Dt). In the next step, the AF-Dt was reacted with salicylaldehyde to yield the imine-functionalized diatomite (IF-Dt). The AF-Dt and IF-Dt were used to support the VO(acac)$_2$ and MoO$_2$(acac)$_2$ complexes, respectively.

FT-IR analysis

The FT-IR spectra of the diatomite nanoparticles in the absence and presence of MSPA are shown in Fig. 1. The infrared spectrum of the pure diatomite (Fig. 1a) indicates a band at 3413 cm^{-1} corresponding to the stretching vibration of hydroxyl groups. Also, the stretching vibration bands of the Si-O-Si groups can be seen in the FT-IR spectrum of the pure diatomite. The higher frequency band at 1084 cm^{-1} is related to v_{asym}, and the

lower one at 791 cm^{-1} is assigned to ν_{sym} of the Si-O-Si groups. The band at 517 cm^{-1} is ascribed to the Si-OH vibrations.[57,58] The FT-IR spectrum of the AF-Dt (Fig. 1b) shows new adsorption bands in the 2800-2950 cm^{-1} region corresponding to the aliphatic -CH$_2$ stretching vibrations of the propyl chain of MSPA. The band at 1618 cm^{-1} is related to the bending vibrations of the NH$_2$ group.[59] These observations reveal that the MSPA is anchored on the surface of the diatomite nanoparticles. The FT-IR spectrum of the IF-Dt (Fig. 1c) exhibits a sharp band at 1633 cm^{-1} corresponding to the imine group.[60] This confirms the formation of the Schiff base compound on the diatomite surface. The two bands appeared at 1496 and 1454 cm^{-1} are ascribed to the aromatic C=C stretching vibrations.[53] The Mo=O and V=O vibration bands usually appear in the 900-1000 cm^{-1} region in the FT-IR spectrum.[56] These bands were not observed in the FT-IR spectra of the V-AF-Dt and Mo-IF-Dt (Fig. 2). It is probably due to the overlapping of these bands with the Si-O vibration bands. However, the FT-IR results confirmed the successful immobilization of the vanadium and molybdenum complexes to the surface of the AF-Dt and IF-Dt, respectively.
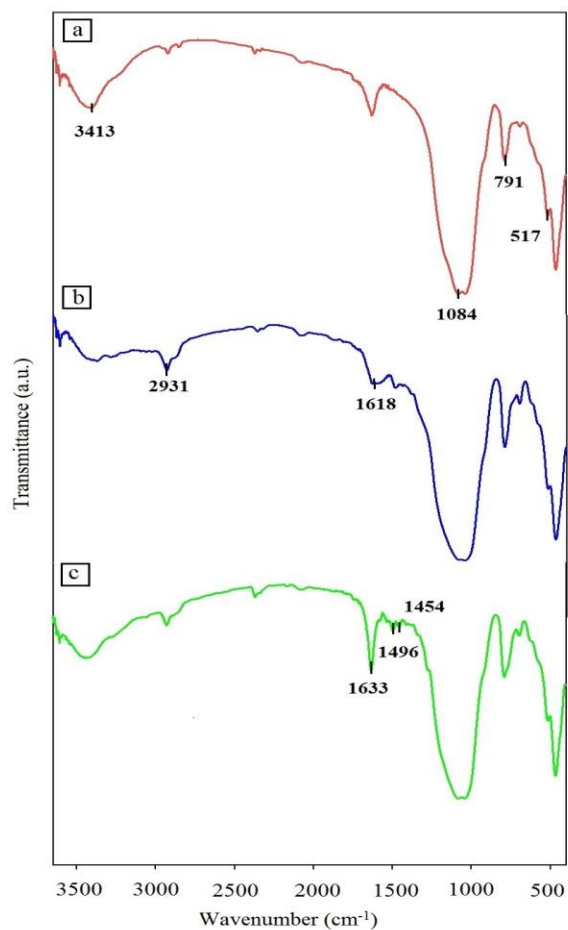

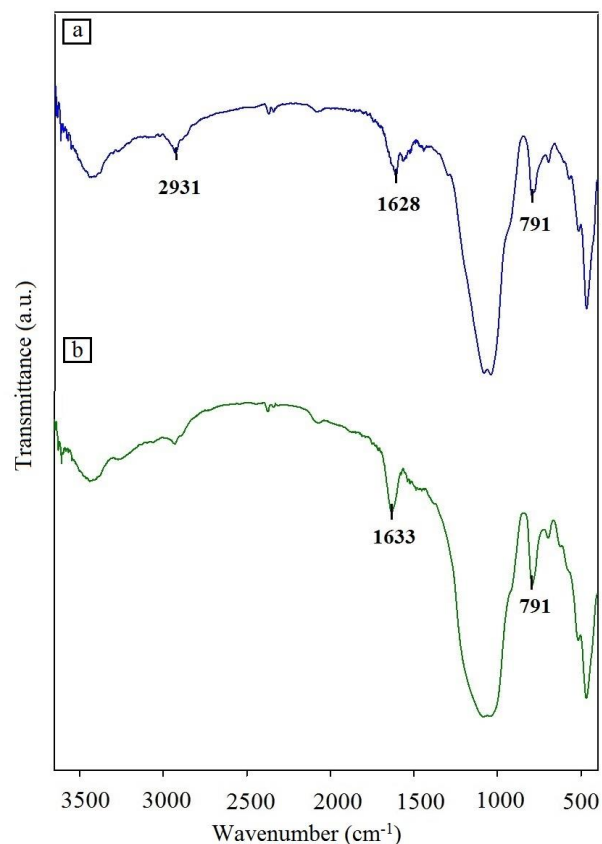**Figure 1.** FT-IR spectra of Dt (a), AF-Dt (b), and IF-Dt (c).

Figure 2. FT-IR spectra of V-AF-Dt (a) and Mo-IF-Dt (b).

PXRD patterns

The PXRD analysis was applied to study the crystalline structure of the pure diatomite, V-AF-Dt, and Mo-IF-Dt. The XRD patterns of the samples are shown in Fig. 3. The results show that the diatomite nanoparticles are formed in a hexagonal phase which corresponds well with the standard crystallographic data for quartz mineral (JCPDS No. 00-046-1045).[61] The main reflections of the crystalline patterns are located at about $2\theta = 22°$, $26°$, $36°$, $39°$, $50°$, and $60°$, which can be perfectly related to the (100), (101), (110), (102), (112), and (211) planes, respectively. The presence of the characteristic peaks in the XRD patterns of the V-AF-Dt and Mo-IF-Dt, and also the comparison of the d values reveal that the crystalline phase of the diatomite particles has not been changed upon immobilization of the vanadium and molybdenum complexes on their surfaces. The average crystallite size of Dt, V-AF-Dt, and Mo-IF-Dt was calculated as 64, 66, and 67 nm, respectively using the Debye-Scherrer equation given below.

$$L = K\lambda/\beta\cos\theta$$

Where K is the Scherrer constant, λ refers to the wavelength of the X-ray beam, β is the full width at half maximum (FWHM) of the peak, and θ is the Bragg angle. The (101) peak was used to estimate the particle sizes.
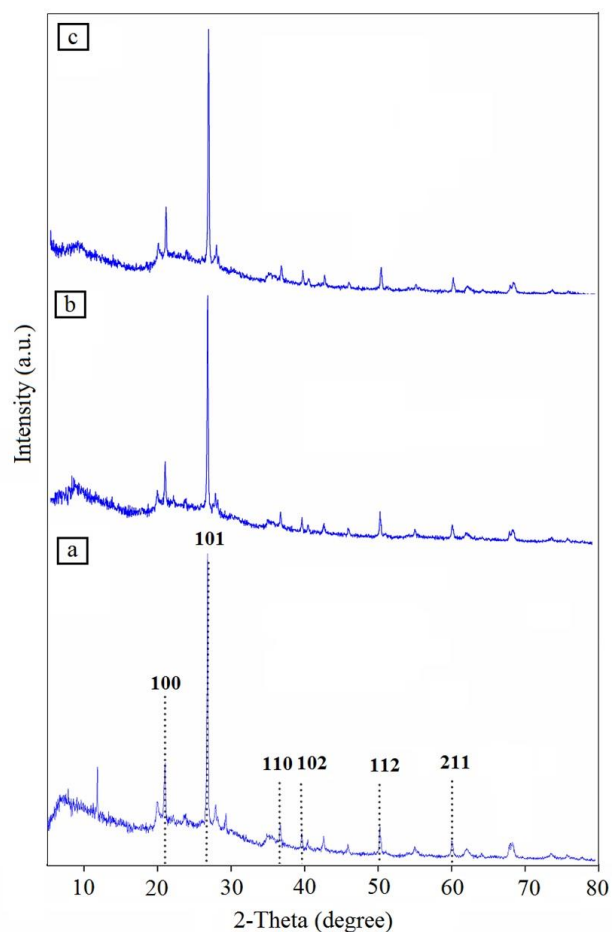
Figure 3. PXRD patterns of Dt (a), V-AF-Dt (b), and Mo-IF-Dt (c).

V(IV) and Mo(VI) complexes onto the surface of the diatomite nanoparticles.
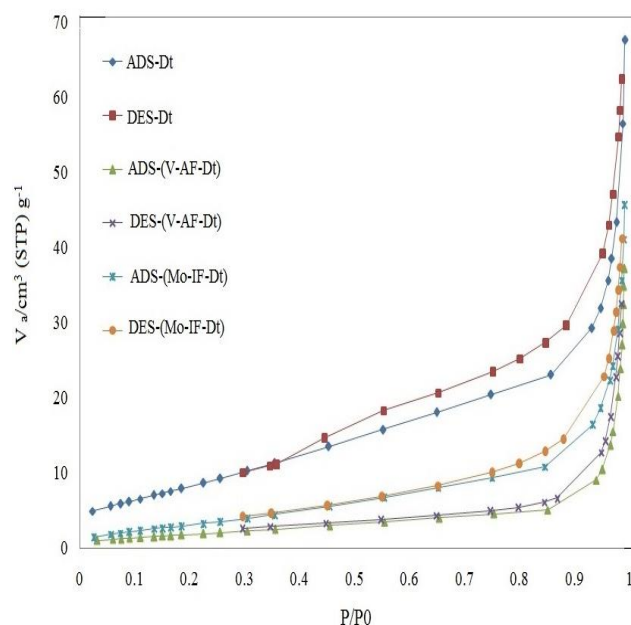

Figure 4. Nitrogen sorption isotherms for Dt, V-AF-Dt, and Mo-IF-Dt.

Table 1. Specific surface area, pore volume, and pore size for Dt, V-AF-Dt, and Mo-IF-Dt

Sample	Specific surface area ($m^2 g^{-1}$)	Pore volume ($cm^3 g^{-1}$)	Pore size (nm)
Dt	29.83	0.097	13.13
Mo-IF-Dt	12.14	0.067	22.12
V-AF-Dt	7.12	0.057	32.15

Nitrogen physisorption

The nitrogen adsorption-desorption isotherms of the Dt, V-AF-Dt, and Mo-IF-Dt samples are shown in Fig. 4. The average pore diameters of the solids were calculated between 2-50 nm, classified as mesoporous materials[62] (Table 1). The results obtained show that the pore diameter for the Dt is smaller than that for the Mo-IF-Di and V-AF-Di. The main reason for these observations is that the porosity on the surface of the diatomite nanoparticles decreases after functionalization. All the samples represent the type V isotherm classified by IUPAC.[63] Another important factor is Brunauer-Emmett-Teller (BET) specific surface area, which was calculated at 29.83, 12.14, and 7.12 $m^2 g^{-1}$ for the Dt, Mo-IF-Dt, and V-AF-Dt, respectively. Moreover, the pore volume of the Dt, Mo-IF-Dt, and V-AF-Dt was measured at 0.097, 0.067, and 0.057 $cm^3 g^{-1}$, respectively. The BET specific surface area and the pore volume of the Dt have been decreased compared to those of the V-AF-Dt and Mo-IF-Dt, which can be related to the immobilization of the

FE-SEM and EDX analysis

The surface morphology and structural feature of the prepared samples were studied by FE-SEM analysis. The FE-SEM images of the V-AF-Dt and Mo-IF-Dt samples exhibit porous particles with a spherical structure of diameter between 60-70 nm (Fig .5). As shown in Fig. 5, the vanadium and molybdenum complexes are successfully immobilized onto the surface of the diatomite nanoparticles.

The EDX analysis was also carried out to confirm the formation of the V-AF-Dt and Mo-IF-Dt compounds (Fig. 6). The peaks corresponding to V, Si, Al, and K elements were observed in the EDX spectrum of the diatomite nanoparticles. The increase in the height of the peak V-Lα in the EDX spectrum of the V-AF-Dt sample is attributed to the immobilization of the $VO(acac)_2$ complex onto the diatomite surface. In the EDX spectrum of the Mo-IF-Dt, in addition to the peaks corresponding to V, Si, Al, and K elements, the peaks related to Mo were also seen. These results confirmed the immobilization of the $MoO_2(acac)_2$ complex onto the diatomite surface.
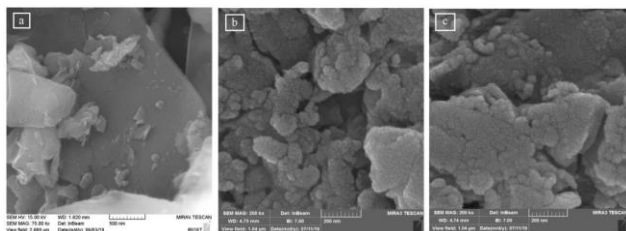
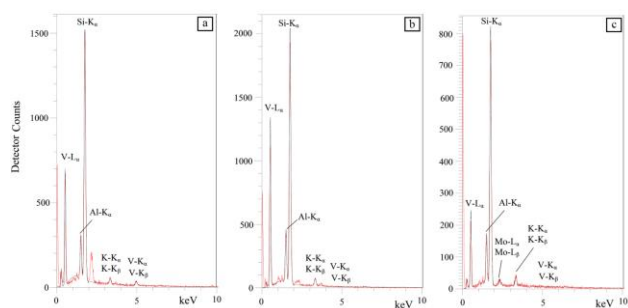**Figure 5.** FE-SEM images of Dt (a), V-AF-Dt (b), and Mo-IF-Dt (c).

Figure 6. EDX analysis of Dt (a), V-AF-Dt (b), and Mo-IF-Dt (c).

Alkene epoxidation catalyzed by V-AF-Dt and Mo-IF-Dt

Since the epoxidation of *cis*-cyclooctene has only one product,[56] it was used as a model reaction to investigate the catalytic activities of the V-AF-Dt and Mo-IF-Dt catalysts. Our tests involved the optimization of different experimental parameters of the model reaction, such as the solvent, oxidant, amount of catalyst, temperature, and time. The results for the epoxidation of *cis*-cyclooctene using TBHP catalyzed by the V-AF-Dt and Mo-IF-Dt catalysts in different solvents are presented in Fig. 7. The solvents with coordinating ability, such as CH_3OH and CH_3CN, can compete with the oxidant to bind to the transition metal centers. Therefore, the observed yield was very low in the presence of these solvents. For both catalytic systems, the 1,2-dichloroethane gave the best yields.
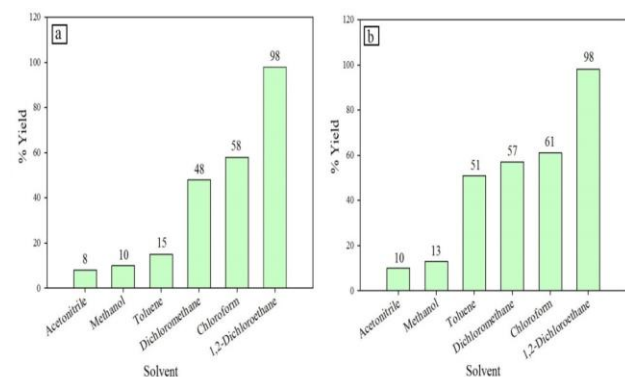

Figure 7. The effect of solvents in the epoxidation of *cis*-cyclooctene catalyzed by V-AF-Dt (a) and Mo-IF-Dt (b) [solvent: 2 ml, *cis*-cyclooctene: 0.5 mmol, TBHP: 1 mmol, catalyst loading: 0.008 mmol (a) and 0.002 mmol (b), reaction time: 180 min (a) and 120 min (b), and temperature: reflux].

The epoxidation of *cis*-cyclooctene was also carried out in the presence of other oxidants such as hydrogen peroxide (H_2O_2) and sodium periodate ($NaIO_4$). For both catalysts, the highest yield of the epoxide product was found in the presence of TBHP as an oxidant (Table 2). The higher activity obtained when using TBHP in comparison with H_2O_2 can be related to the weaker O-O bonds of TBHP, which make it an efficient oxidant. Moreover, the epoxidation of *cis*-cyclooctene using TBHP did not proceed in the absence of the catalysts under mild conditions.

Table 2. The effect of oxidant on the epoxidation of *cis*-cyclooctene[a]

Solvent	Oxidant	Yield (%)[b]	
		V-AF-Dt	**Mo-IF-Dt**
	TBHP	0	0
CH_3CN	H_2O_2	31	38
	$NaIO_4$	0	0
	TBHP	98	98
$C_2H_4Cl_2$	H_2O_2	6	5
	$NaIO_4$	0	0

[a]Reaction conditions: [$C_2H_4Cl_2$: 2 ml, *cis*-cyclooctene: 0.5 mmol, oxidant: 1 mmol, catalyst loading: 0.008 mmol (V-AF-Dt) and 0.002 mmol (Mo-IF-Dt), reaction time: 180 min (V-AF-Dt) and 120 min (Mo-IF-Dt), and temperature: 85 °C]. [b]GLC yields are based on the starting cyclooctene.

As another parameter, the effect of the reaction time on the epoxidation of *cis*-cyclooctene using TBHP was studied (Fig. 8). The results show that the Mo-IF-Dt is more reactive than the V-AF-Dt catalyst. For the Mo-IF-Dt catalyst, the epoxide yield reaches a maximum after 120 min and then becomes constant, while the V-AF-Dt catalyst needs 180 min to accomplish this goal.
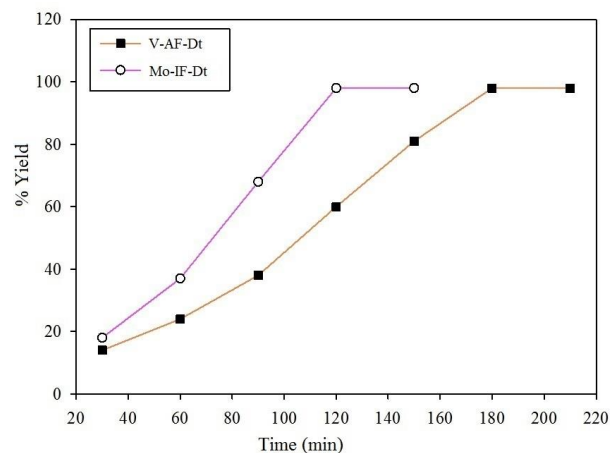

Fig. 8. The effect of the reaction time in the epoxidation of *cis*-cyclooctene catalyzed by V-AF-Dt and Mo-IF-Dt [$C_2H_4Cl_2$: 2 ml, *cis*-cyclooctene: 0.5 mmol, TBHP: 1 mmol, catalyst loading: 0.008 mmol (V-AF-Dt) and 0.002 mmol (Mo-IF-Dt), and temperature: 85 °C].

Figure 9 illustrates the effect of the amount of catalyst in the epoxidation of *cis*-cyclooctene. The results show that

by increasing the amount of the Mo-IF-Dt and V-AF-Dt catalysts up to 10 mg (0.002 mmol) and 20 mg (0.006 mmol), respectively, the epoxide yield increases and then becomes constant. In addition, a blank system with no catalyst was tested that proved using the catalyst was necessary to proceed the reaction.
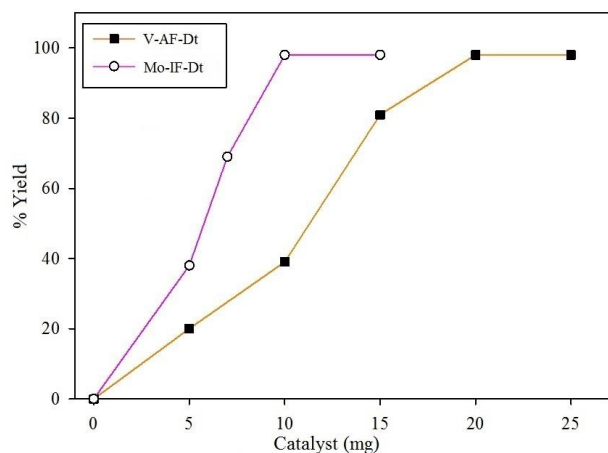

Figure 9. The effect of the amount of catalyst in the epoxidation of *cis*-cyclooctene catalyzed by V-AF-Dt and Mo-IF-Dt [$C_2H_4Cl_2$: 2 ml, *cis*-cyclooctene: 0.5 mmol, TBHP: 1 mmol, reaction time: 180 min (V-AF-Dt) and 120 min (Mo-IF-Dt), and temperature: 85 °C].

The oxidant/substrate molar ratio is one of the most important parameters in catalytic epoxidation procedures. As shown in Fig. 10, the optimum oxidant/substrate molar ratio for both catalysts was found to be 2. For both catalysts, increasing the ratio from 2 to 3 does not change the epoxidation yields considerably while decreasing it to 1 reduces the yields significantly.
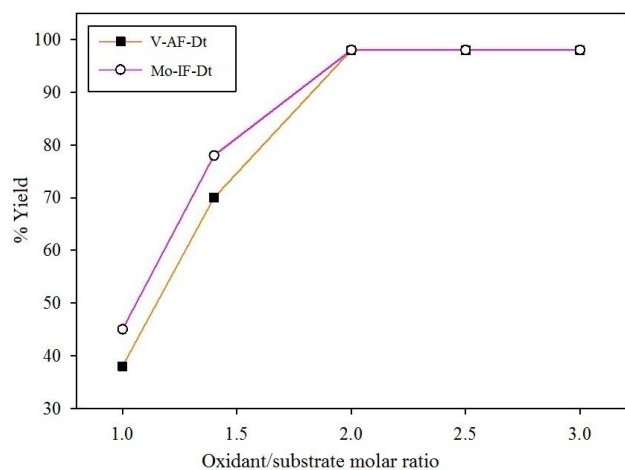

Fig. 10. The effect of the oxidant/substrate molar ratio in the epoxidation of *cis*-cyclooctene catalyzed by V-AF-Dt and Mo-IF-Dt [$C_2H_4Cl_2$: 2 ml, catalyst loading: 0.006 mmol (V-AF-Dt) and 0.002 mmol (Mo-IF-Dt), reaction time: 180 min (V-AF-Dt) and 120 min (Mo-IF-Dt), and temperature: 85 °C].

Moreover, the effect of the reaction temperature on the epoxidation yield was studied at four different temperatures (25, 45, 65, and 85 °C), keeping the other parameters fixed (Fig. 11). For both catalysts, the best epoxide yields were obtained at 85 °C.
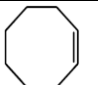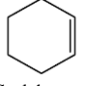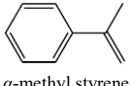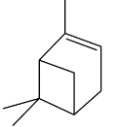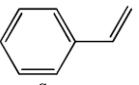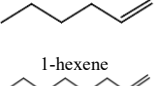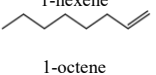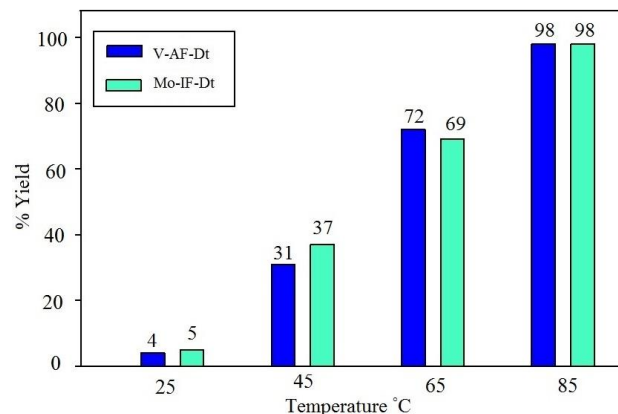

Fig. 11. The effect of the reaction temperature in the epoxidation of *cis*-cyclooctene catalyzed by V-AF-Dt and Mo-IF-Dt [$C_2H_4Cl_2$: 2 ml, *cis*-cyclooctene: 0.5 mmol, TBHP: 1 mmol, catalyst loading: 0.006 mmol (V-AF-Dt) and 0.002 mmol (Mo-IF-Dt), and reaction time: 180 min (V-AF-Dt) and 120 min (Mo-IF-Dt)].

Since the epoxidation of *cis*-cyclooctene using the new catalysts showed high efficiency, their catalytic activities for epoxidation of other linear and cyclic alkenes were also studied (Table 3). The results show that the catalytic epoxidation of the cyclic alkenes needs a shorter reaction time than the linear ones. The probable reason for this is that the electron density of the cyclic alkenes is higher than the linear ones, which facilitates access to the oxidant with a high electron affinity. For both catalysts, the cyclohexene showed a lower epoxidation yield in comparison to cyclooctene. These observations can be due to some cyclooctene conformations that decrease the activation energy of the reaction.[64] The α-methyl styrene was more reactive than styrene. This can be related to its more electron density because of the existence of the electron-donating methyl group connected to the ring. The linear alkenes, 1-hexene and 1-octene, showed lower epoxide yields (Table 3, entries 6 and 7). In both catalytic systems, the conversion of 1-hexene was higher than that for 1-octene, which can be related to a more steric hindrance around 1-octene.[53]

We also compared the catalytic activities of the prepared immobilized catalysts (V-AF-Dt and Mo-IF-Dt) with the corresponding homogeneous VO(acac)$_2$ and MoO$_2$(acac)$_2$ complexes in the epoxidation of *cis*-cyclooctene under the optimized reaction conditions (Table 4). The results showed that the immobilization of VO(acac)$_2$ and MoO$_2$(acac)$_2$ complexes onto AF-Dt and IF-Dt increases the catalytic activity and the selectivity for the corresponding epoxide.

Table 3. Epoxidation of some alkenes using TBHP catalyzed by V-AF-Dt and Mo-IF-Dt catalysts[a]

Entry	Alkene	V-AF-Dt		Mo-IF-Dt	
		Time (min)	Yield (%)[b]	Time (min)	Yield (%)[b]
1	cis-cyclooctene	180	98	120	98
2	Cyclohexene	180	93	120	94
3	α-methyl styrene	180	82	120	88
4	α-Pinene	180	81	180	87
5	Styrene	360	75	240	81
6	1-hexene	360	52	240	61
7	1-octene	360	48	240	56

[a]Reaction conditions: [C$_2$H$_4$Cl$_2$: 2 mL, cis-cyclooctene: 0.5 mmol, TBHP: 1 mmol, catalyst loading: 0.006 mmol (V-AF-Dt) and 0.002 mmol (Mo-IF-Dt), and temperature: 85 °C]. [b]GLC yields are based on the starting alkenes.

Table 4. Comparison between the catalytic activities of V-AF-Dt, Mo-IF-Dt, VO(acac)$_2$, and MoO$_2$(acac)$_2$ in the epoxidation of cis-cyclooctene[a]

Catalyst	Epoxide yield (%)[b]
VO(acac)$_2$	73
V-AF-Dt	98
MoO$_2$(acac)$_2$	68
Mo-IF-Dt	98

[a]Reaction conditions: [C$_2$H$_4$Cl$_2$: 2 ml, cis-cyclooctene: 0.5 mmol, TBHP: 1 mmol, reaction time: 180 min (V-AF-Dt) and 120 min (Mo-IF-Dt), and temperature: 85 °C]. [b]GLC yields are based on the starting cyclooctene.

Based on our previous report, a probable mechanism can be proposed for the epoxidation of cis- cyclooctene by the V-AF-Dt and Mo-IF-Dt catalysts (Scheme 2).[53] During a catalytic cycle, the hydroxyl proton of TBHP transfers to a terminal oxygen atom of the metal-oxo complex, which results in the coordination of the *tert*-butylperoxide anion to the Lewis acidic metal centers. Then the alkene is coordinated to the metal center and, as a nucleophile, is inserted into the metal-oxygen bond of the coordinated peroxide electrophile anion. In the next step, the epoxide product is generated, and the *tert*-butylperoxide anion is converted to the tert-butoxide anion. According to this mechanism, the electron-rich olefins can facilitate the

epoxidation reaction compared with the electron-poor ones.
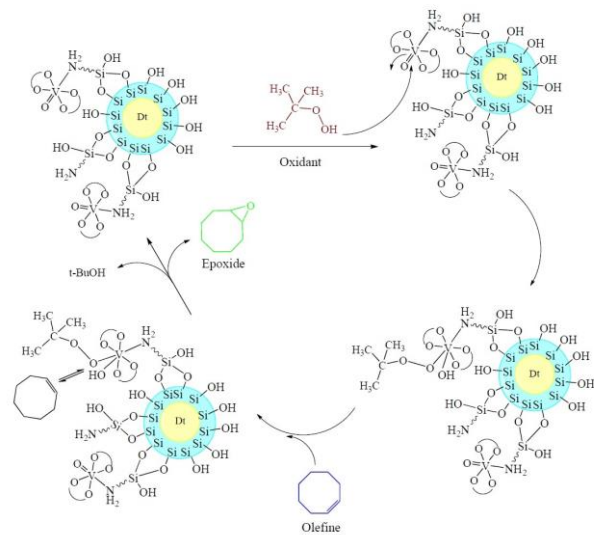
Scheme 2. Proposed mechanism for the epoxidation of alkenes with TBHP catalyzed by V-AF-Dt

These new catalytic systems were compared with other heterogeneous catalytic systems containing molybdenum and vanadium metal centers (Table 5). As given in Table 5, the Mo-IF-Dt/TBHP catalytic system displays a higher turn-over frequency (TOF) than the V-AF-Dt/TBHP system. Compared to other catalysts, the Mo-IF-Dt is superior in terms of catalyst loading and TOF.

Table 5. Comparison of the results obtained for the epoxidation of cis-cyclooctene catalyzed by V-AF-Dt and Mo-IF-Dt catalysts with other reported heterogeneous catalytic systems containing Mo and V metal centers

Catalyst	Catalyst loading (mmol)	Time (h)	Yield (%)	Amount of cyclooctene (mmol)	TOF (h^{-1})	Ref.
Sep-Am-MoO$_2$	0.0074	1.25	98	0.7	74.16	56
Mo-Im-BNPs	0.0064	1	97	0.5	126	59
MoO$_2$salen-SBA-15	0.0026	8	4.1	5	10	65
Mo-IF-Dt	0.0026	2	98	0.5	94.23	This work
V-en-BNPs	0.0132	1	95	0.5	60	59
Fe@B-N-V	0.0020	4.5	98	0.5	55	54
Fe@B-Im-V	0.0112	0.75	98	0.5	58	54
V-AFBNPs	0.0056	3	93	0.7	39	55
V-AF-Dt	0.0064	3	98	0.5	25.52	This work

Catalyst recovery and reuse

The new heterogeneous catalysts were recovered and reused several times. The results showed few or no decrease in the product yield even after three runs (Table 6). This can be related to the strong binding of the metal centers to the amine and imine-functionalized diatomite, which kept connected even after washing. The

reason for the gradual decrease in the yields is the separation of metals from the diatomite surface.

Table 6. Epoxidation of *cis*-cyclooctene with TBHP using recycled catalysts[a]

Catalyst	Number of cycles	Epoxide yield (%)[b]	TOF (h^{-1})[c]	Metal leached (%)[d]	Content (mmol g^{-1})[e]
V-AF-Dt	1	98	25.52	ND	0.32
	2	96	25	ND	0.32
	3	92	23.95	ND	0.31
	4	90	23.43	ND	0.29
Mo-IF-Dt	1	98	94.23	ND	0.26
	2	97	93.26	ND	0.26
	3	96	92.30	ND	0.25
	4	92	88.46	ND	0.23

[a]Reaction conditions: [C$_2$H$_4$Cl$_2$: 2 ml, *cis*-cyclooctene: 0.5 mmol, TBHP: 1 mmol, reaction time: 180 min (V-AF-Dt) and 120 min (Mo-IF-Dt), and temperature: 85 °C]. [b]GLC yields are based on the starting cyclooctene. [c]TOF = (mole of reactant) (yield)/(mole of catalyst)(time). [d]Determined by ICP analysis. ND: not detected. [e]Metal content of the recycled catalyst.

5. CONCLUSIONS

In summary, two new catalysts were prepared by anchoring VO(acac)$_2$ and MoO$_2$(acac)$_2$ precursor complexes onto the surface of amine and imine-functionalized diatomite nanoparticles. Immobilization of VO(acac)$_2$ and MoO$_2$(acac)$_2$ complexes onto diatomite nanoparticles, as an insoluble inorganic carrier, can improve their catalytic efficiency. The prepared catalysts exhibited good catalytic activity in the epoxidation of different alkenes using TBHP as an oxidant. The results showed that the Mo-IF-Dt/TBHP catalytic system was more reactive than the V-AF-Dt/TBHP system. Compared with other reported heterogeneous catalytic systems containing Mo and V metal centers, our catalytic systems are superior in cost, reaction time, catalyst loading, epoxide yield, and turn-over frequency (TOF). The type of solvent is one of the most important factors that influence the efficiency of the catalytic system. In both catalytic systems, 1,2-dichloroethane as an aprotic, non-polar, and hydrophobic solvent gave the best results.

CONFLICTS OF INTEREST

There is no conflict of interest to declare.

ACKNOWLEDGEMENTS

AUTHOR INFORMATION

Corresponding Author
Bahram Bahramian: Email: bahramian.b@shahroodut.ac.ir, *ORCID*: 0000-0003-4671-3869

Author(s)
Sahar Asadi, Vahid Mirdarvatan

REFERENCES

1. M. Mirzaee, B. Bahramian, A. Ashrafian, A. Amoli, *Appl. Organomet. Chem.* **2018**, *32*, 1-9.
2. P. D. Oldenburg, R. Mas-Ballesté, L. Que, *Mech. Homog. Heterog. Epoxidation Catal.* **2008**, 451-469.
3. S. Goswami, S. Singha, R. Saha, A. Singha Roy, M. Islam, S. Kumar, *Inorganica Chim. Acta.* **2019**, *486*, 352-360.
4. W. Jiang, J. D. Gorden, C. R. Goldsmith, *Inorg. Chem.* **2012**, *51*, 2725-2727.
5. M. F. I. Al-Hussein, M. S. S. Adam, *Appl. Organomet. Chem.* **2020**, *34*, 1-22.
6. Z. Asgharpour, F. Farzaneh, A. Abbasi, *RSC Adv.* **2016**, *6*, 95729-95739.
7. S. Bhunia, S. Koner, *Polyhedron.* **2011**, *30*, 1857-1864.
8. S. Ghiami, M. A. Nasseri, A. Allahresani, M. Kazemnejadi, *React. Kinet. Mech. Catal.* **2019**, *126*, 383-398.
9. M. Kazemnejadi, B. Mahmoudi, Z. Sharafi, M. A. Nasseri, A. Allahresani, M. Esmaeilpour, *J. Organomet. Chem.* **2019**, *896*, 59-69.
10. Y. Shen, P. Jiang, P. T. Wai, Q. Gu, W. Zhang, *Catalysts.* **2019**, *9*, 31.
11. Z. Li, S. Wu, D. Zheng, J. Liu, H. Liu, H. Lu, Q. Huo, J. Guan, Q. Kan, *Appl. Organomet. Chem.* **2014**, *28*, 317-323.
12. Y. Leng, J. Liu, C. Zhang, P. Jiang, *Catal. Sci. Technol.* **2014**, *4*, 997-1004.
13. L. Bai, K. Li, Y. Yan, X. Jia, J.M. Lee, Y. Yang, *ACS Sustain. Chem. Eng.* **2016**, *4*, 437-444.
14. F. Farzaneh, Y. Sadeghi, M. Maghami, Z. Asgharpour, *J. Clust. Sci.* **2016**, *27*, 1701-1718.
15. H. Kargar, M. Bazrafshan, M. Fallah-Mehrjardi, R. Behjatmanesh-Ardakani, H. A. Rudbari, K. S. Munawar, M. Ashfaq, M. N. Tahir, *Polyhedron.* **2021**, *202*, 115194.
16. H. Kargar, P. Forootan, M. Fallah-Mehrjardi, R. Behjatmanesh-Ardakani, H. A. Rudbari, K. S. Munawar, M. Ashfaq, M. N. Tahir, *Inorganica Chim. Acta.* **2021**, *523*, 120414.
17. H. Kargar, M. Fallah-Mehrjardi, *Inorg. Chem. Res.* **2021**, *5*, 201-206.
18. M. R. Maurya, M. Kumar, S. J. J. Titinchi, H. S. Abbo, S. Chand, *Catal. Letters.* **2003**, *86*, 97-105.
19. H. Kargar, A. Moghimi, M. Fallah-Mehrjardi, R. Behjatmanesh-Ardakani, H. A. Rudbari, K. S. Munawar, *J. Sulfur Chem.* **2022**, *43*, 22-36.
20. R. Kia, H. Kargar, *J. Coord. Chem.* **2015**, *68*, 1441-1451.
21. M. Sutradhar, L. M. D. R. S. Martins, M. F. C. Guedes da Silva, A. J. L. Pombeiro, *Coord. Chem. Rev.* **2015**, *301*, 200-239.
22. Z. Li, S. Wu, Y. Ma, H. Liu, J. Hu, L. Liu, Q. Huo, J. Guan, Q. Kan, *Transit. Met. Chem.* **2013**, *38*, 243-251.
23. P. Zahajská, S. Opfergelt, S. C. Fritz, J. Stadmark, D.

J. Conley, *Quaternary Research* , **2020**, *96*, 48-52.

24. H. A. Alyosef, S. Ibrahim, J. Welscher, A. Inayat, A. Eilert, R. Denecke, W. Schwieger, T. Münster, G. Kloess, W.D. Einicke, D. Enke, *Int. J. Miner. Process.* **2014**, *132*, 17-25.

25. Z. Han, C. Wang, X. Zou, T. Chen, S. Dong, Y. Zhao, J. Xie, H. Liu, *Appl. Surf. Sci.* **2020**, *502*, 144201.

26. A. M. Rabie, M. Shaban, M. R. Abukhadra, R. Hosny, S. A. Ahmed, N. A. Negm, *J. Mol. Liq.* **2019**, *279*, 224-231.

27. Y. Tan, C. Li, Z. Sun, R. Bian, X. Dong, X. Zhang, S. Zheng, *Chem. Eng. J.* **2020**, *388*, 124386.

28. N. Caliskan, A. R. Kul, S. Alkan, E. G. Sogut, I. Alacabey, *J. Hazard. Mater.* **2011**, *193*, 27-36.

29. Z. Ren, H. Gao, H. Zhang, X. Liu, *Int. J. Miner. Process.* **2014**, *130*, 28-33.

30. N. Ediz, I. Bentli, I. Tatar, *Int. J. Miner. Process.* **2010**, *94*, 129-134.

31. X. Li, C. Bian, W. Chen, J. He, Z. Wang, N. Xu, G. Xue, *Appl. Surf. Sci.* **2003**, *207*, 378-383.

32. F. R. Lamastra, S. Mori, V. Cherubini, M. Scarselli, F. Nanni, *Mater. Chem. Phys.* **2017**, *194*, 253-260.

33. S. É. Ivanov, A. V. Belyakov, *Glas. Ceram.* **2008**, *65*, 48-51.

34. Y. Du, H. Fan, L. Wang, J. Wang, J. Wu, H. Dai, *J. Mater. Chem. A.* **2013**, *1*, 7729-7737.

35. Y. Li, H. Xiao, M. Chen, Z. Song, Y. Zhao, *J. Mater. Sci.* **2014**, 49, 6696-6704.

36. W. Yu, L. Deng, P. Yuan, D. Liu, W. Yuan, P. Liu, H. He, Z. Li, F. Chen, *J. Colloid Interface Sci.* **2015**, *448*, 545-552.

37. H. Liu, Y. Zhao, Y. Zhou, L. Chang, J. Zhang, *Sci. Total Environ.* **2019**, *652*, 651-659.

38. S. Karaman, A. Karaipekli, A. Sar, A. Biçer, *Sol. Energy Mater. Sol. Cells.* **2011**, *95*, 1647-1653.

39. J. Li, D. huai Tu, Y. Li, W. Wang, Q. Yu, J. Yang, J. Lu, *Appl. Catal. A Gen.* **2018**, *549*, 112-116.

40. C. J. Yue, S. S. Yao, L. P. Gu, *J. Porous Mater.* **2015**, *22*, 455-464.

41. H. Liu, G. Lu, Y. Guo, Y. Guo, J. Wang, *Catal. Today.* **2004**, *93*, 353-357.

42. M. Sun, W. C. Chen, L. Zhao, X. L. Wang, Z. M. Su, *Inorg. Chem. Commun.* **2018**, *87*, 30-35.

43. Q. Li, G. Zhai, Y. Xu, T. Odoom-Wubah, L. Jia, J. Huang, D. Sun, Q. Li, *Ind. Eng. Chem. Res.* **2019**, *58*, 14008-14015.

44. C. Huang, H. Zhang, Y. Zhao, S. Chen, Z. Liu, *J. Colloid Interface Sci.* **2012**, *386*, 60-65.

45. Z. Zhang, Z. Wang, *J. Org. Chem.* **2006**, *71*, 7485-7487.

46. C. Hao, X. Zhao, *Adv. Mater. Res.* **2010**, *113*, 1824-1827.

47. B. Bahramian, M. Bakherad, A. Keivanloo, Z. Bakherad, B. Karrabi, *Appl. Organomet. Chem.* **2011**, *25*, 420-423..

48. G. Zhang, Z. Sun, Y. Duan, R. Ma, S. Zheng, *Appl. Surf. Sci.* **2017**, *412*, 105-112.

49. S. K. Padmanabhan, S. Pal, E. Ul Haq, A. Licciulli, *Appl. Catal. A Gen.* **2014**, *485*, 157-162.

50. R. Zuo, G. Du, W. Zhang, L. Liu, Y. Liu, L. Mei, Z. Li, *Adv. Mater. Sci. Eng.* **2014**.

51. Z. Jia, T. Li, Z. Zheng, J. Zhang, J. Liu, R. Li, Y. Wang, X. Zhang, Y. Wang, C. Fan, *Chem. Eng. J.* **2020**, *380*, 122422.

52. Bahramian, F. D. Ardejani, V. Mirkhani, K. Badii, *Appl. Catal. A Gen.* **2008**, *345*, 97-103.

53. M. Mirzaee, B. Bahramian, M. Shahraki, H. Moghadam, A. Mirzaee, *Catal. Letters.* **2018**, *148*, 3003-3017.

54. M. Mirzaee, B. Bahramian, P. Gholampour, S. Teymouri, T. Khorsand, *Appl. Organomet. Chem.* **2019**, *33*, 1-14.

55. M. Mirzaee, B. Bahramian, M. Mirebrahimi, *Chinese J. Catal.* **2016**, *37*, 1263-1274.

56. A. Golmohamadpour, B. Bahramian, A. Shafiee, L. Ma'mani, *Mater. Chem. Phys.* **2018**, *218*, 326-335.

57. P. Yuan, D. Liu, D. Y. Tan, K. K. Liu, H. G. Yu, Y. H. Zhong, A. H. Yuan, W. Bin Yu, H. P. He, *Microporous Mesoporous Mater.* **2013**, *170*, 9-19.

58. P. Yuan, D. Yang, Z. Lin, H. He, X. Wen, L. Wang, F. Deng, *J. Non. Cryst. Solids.* **2006**, *352*, 3762-3771.

59. M. Mirzaee, B. Bahramian, J. Gholizadeh, A. Feizi, R. Gholami, *Chem. Eng. J.* **2017**, *308*, 160-168.

60. Z. Salarvand, M. Amirnasr, S. Meghdadi, *J. Lumin.* **2019**, *207*, 78-84.

61. J. Glinnemann, H. E. King Jr, H. Schulz, Th. Hahn, S. J. La Placa, F. Dacol, *Z. Kristallogr. Krist.* **1992**, *198*, 177-212.

62. M. Manzano, M. Vallet-Regí, *Adv. Funct. Mater.* **2020**, *30*, 3-5.

63. J. Rouquerol, F. Rouquerol, P. Llewellyn, G. Maurin, K. S. Sing, Adsorption by powders and porous solids: principles, methodology and applications, Academic press, **2013**.

64. M. Bagherzadeh, M. Zare, T. Salemnoush, S. Özkar, S. Akbayrak, *Appl. Catal. A Gen.* **2014**, *475*, 55-62.

65. Y. Yang, S. Hao, Y. Zhang, Q. Kan, *Solid State Sci.* **2011**, *13*, 1938-1942.